Principles of 3D Turntable Radar Imaging

Timothy P. Ray, Jaime X. Lopez, and Zhijun Qiao,
Department of Mathematics, University of Texas-Pan American,
1201 W. University Dr., Edinburg, TX 78539 USA
Email: qiao@utpa.edu

***Abstract*—**
In this paper, a filtered adjoint inversion scheme for turntable inverse synthetic aperture radar (ISAR) data is derived for three spatial dimensions from a scalar wave equation model. The proposed data inversion scheme motivates the use of filtered back projection (FBP) and convolution back projection (CBP) imaging algorithms. This paper also provides a derivation of a general imaging filter needed for accurate near-field FBP and CBP imaging algorithms, which will be shown to reduce to familiar results found in SWISAR (Spherical-Wave ISAR) imaging.

***Index Terms*—Inverse Synthetic Aperture Radar, Near-Field Imaging, Fourier Diffraction Theorem, Turntable Radar, Filtered Back-Projection, Convolution Back Projection, Radar Tomography**

I. INTRODUCTION

Inverse Synthetic Aperture Radar (ISAR) is a high-resolution imaging system that consists of both a real-aperture radar system and a moving target scene. An ISAR system uses a set of stationary antennas to emit a sequence of short energy bursts, and to take scattering measurements in the presence of a moving target scene. There are many works on the fundamental principles of ISAR imaging [1], [5], [13], [18], in which it has been shown that both two-dimensional and three-dimensional image formation is possible for targets undergoing either rotational or translational motion. Efficient near-field algorithms [3], [10], [25] for processing ISAR data have also been proposed for two and three-dimensional imaging, which can be derived via the filtered adjoint inversion approach proposed in this paper.

In this paper the the problem of image formation is primarily considered in terms of ISAR, but Turntable Radar is different from many ISAR applications where the physical geometry is unknow. For this reason it can be usefull to study this problem in terms of Spotlight-Mode SAR [4], [12].

In section II, the general ISAR received signal for start-stop turntable setups is first derived from a scalar wave equation model. The scalar wave model used in the paper is derived from Maxwell's equations by using a first-order Born approximation [2]. A short review of far-field radar imaging is included beginning with the derivation of the Fourier diffraction theorem in radar imaging, which relates the ISAR received signal S to the Fourier transform of the target reflectivity function V. The Fourier Diffraction theorem (FDT)[9] provides the basis for most FFT radar imaging algorithms. The derivation of the FDT is followed by a quick discussion of the forward model for turntable ISAR data in two and three dimensions.

In section IV the general ISAR received signal, S, is first written in terms of a Fourier integral operator (FIO), $S = FV$, in which it will be noted that the ISAR signal in the frequency domain is a function on the unit cylinder C^m, where $m = 2, 3$ depending on system configuration. The formal adjoint of the forward ISAR FIO on $L^2(C^m)$ is then derived for both two and three dimensions on the basis of a filtered back projection ISAR imaging algorithm via $V = F^\dagger \mathcal{Q} F V$. In the case of turntable ISAR, applying the back projection operator does not result in an exact inversion of the data, which actually requires evaluating an appropriate data filter $\mathcal{Q}$. The filter $\mathcal{Q}$ is determined by using the stationary phase method.

II. THE FORWARD PROBLEM

In radar imaging applications the received signal is a recorded measurement of a scattered electromagnetic field. For this reason, the ideal mathematical model for radar imaging would be that found in Maxwell's equations for the electromagnetic field. We will use the following scalar-wave equation model for radar imaging which can be deduced from Maxwell's equations under a weak-scattering assumption[16]:

$$\left(\nabla^2 + k^2\right) U^{\text{in}}(f, \mathbf{x}) = -J(f, \mathbf{x}), \tag{1a}$$

$$\left(\nabla^2 + k^2\right) U^{\text{sc}}(f, \mathbf{x}) = -V(\mathbf{x}) U^{\text{in}}(f, \mathbf{x}), \tag{1b}$$

where $\mathbf{x} = (x_1, x_2, x_3) \in \mathbb{R}^3$, $k = 2\pi f/c$ and c is the speed of light in a vacuum. The scalar quantities U^{in} and U^{sc} denote the incident and scattered fields, respectively. The quantity J[1]denotes the source due to signal transmission, and V is the complex-valued target reflectivity function. We will assume that the quantities U^{in}, U^{sc} and J are square-integrable in the frequency variable, f, so that their corresponding inverse Fourier transforms, u^{in}, u^{sc} and j, exist in the time variable t. This assumption allows us to refer to the following time domain version of (1):

$$\left(\nabla^2 - \frac{1}{c_0^2}\partial_t^2\right) u^{\text{in}}(t, \mathbf{x}) = -j(t, \mathbf{x}), \tag{2a}$$

$$\left(\nabla^2 - \frac{1}{c_0^2}\partial_t^2\right) u^{\text{sc}}(t, \mathbf{x}) = -V(\mathbf{x}) u^{\text{in}}(t, \mathbf{x}), \tag{2b}$$

According to this scalar model the scattered field depends on the incident field, which depends on the source due to

[1]The source term J does not directly correspond to the current density function $\mathbf{J}$, but is related to both $\mathbf{J}$ and the charge density function ρ by $[J_i] = \frac{1}{\epsilon_0}\nabla\rho + i\omega\boldsymbol{\mu}_0\mathbf{J}$ for the field $\mathbf{E}$ field and $[J_i] = -\nabla \times \mathbf{J}$ for the $\mathbf{H}$ field.

978-1-4673-0658-4/12/$31.00 ©2012 IEEE

transmission. Thus, in order to come up with an explicit expression for the received signal, we can begin by re-writing the source term j in (2a) in terms of the transmitted signal $p(t)$. Here we will assume that the transmitter radiates isotropically and is centered at $\mathbf{x}_0 \in \mathbb{R}^3$ so that we can write $j(t,\mathbf{x}) = p(t)\delta(\mathbf{x}-\mathbf{x}_0)$. Consequently the received signal, assuming a mono-static setup, is given by

$$s(t) \equiv u^{\text{sc}}(t,\mathbf{x}_0) = \int_{\mathbb{R}^3} V(\mathbf{z}) \frac{p\left(t - \frac{2|\mathbf{z}-\mathbf{x}_0|}{c_0}\right)}{(4\pi)^2 |\mathbf{z}-\mathbf{x}_0|^2} d\mathbf{z}, \quad (3)$$

or in the frequency domain:

$$S(f) = P(f) \int_{\mathbb{R}^3} V(\mathbf{z}) \frac{e^{-i2k|\mathbf{z}-\mathbf{x}_0|}}{(4\pi)^2 |\mathbf{z}-\mathbf{x}_0|^2} d\mathbf{z}, \quad (4)$$

A. The Fourier Diffraction Theorem in ISAR Imaging

Many ISAR imaging systems are set up so that distances to targets are considerably large. In these cases it is quite useful to employ some sort of far-field approximation to aid in the analysis of the imaging problem. Note that the range from the antenna located at $\mathbf{x}_0$ on the transmitter to that target located at $\mathbf{z}$ is given by:

$$|\mathbf{z}-\mathbf{x}_0| = |\mathbf{x}_0| - \widehat{\mathbf{x}_0}\cdot\mathbf{z} + O\left(\frac{|\mathbf{z}|^2}{|\mathbf{x}_0|}\right) \quad (5)$$

We find that we can rewrite the integrand of the integral in (4) as:

$$\begin{aligned} V(\mathbf{z})\frac{e^{-i2k|\mathbf{z}-\mathbf{x}_0|}}{(4\pi)^2|\mathbf{z}-\mathbf{x}_0|^2} &= V(\mathbf{z})\frac{e^{-i2k|\mathbf{x}_0|}}{(4\pi)^2|\mathbf{x}_0|^2} e^{i2k\widehat{\mathbf{x}_0}\cdot\mathbf{z}} \\ \left(1+O\left(\frac{|\mathbf{z}|}{|\mathbf{x}_0|}\right)\right)&\left(1+O\left(\frac{k|\mathbf{z}|^2}{|\mathbf{x}_0|}\right)\right) \end{aligned} \quad (6)$$

Thus, if we make the assumption that $|\mathbf{z}|, k|\mathbf{z}|^2 << |\mathbf{x}_0|$, then our far-field version of the received signal is given by:

$$\begin{aligned} S(f) &= P(f)\frac{e^{-i2k|\mathbf{x}_0|}}{(4\pi)^2|\mathbf{x}_0|^2}\int_{\mathbb{R}^3} V(\mathbf{z}) e^{i2k\widehat{\mathbf{x}_0}\cdot\mathbf{z}} d\mathbf{z} \\ &= P(f)\frac{e^{-i2k|\mathbf{x}_0|}}{(4\pi)^2|\mathbf{x}_0|^2}\mathcal{F}\{V\}(-2k\widehat{\mathbf{x}_0}). \end{aligned} \quad (7)$$

Many radar imaging algorithms employ a matched-filtering step to recover the set of range profiles, d, whose spectrum, D, is given by:

$$\begin{aligned} D(f) &= (4\pi)^2|\mathbf{x}_0|^2 e^{i2k|\mathbf{x}_0|}\overline{P(f)}S(f) \\ &= |P(f)|^2 \mathcal{F}\{V\}(-2k\widehat{\mathbf{x}_0}) \end{aligned} \quad (8)$$

where $\overline{P}$ denotes the complex conjugate of P. The actual matched-filtering step is implemented by multiplying each individual ISAR signal S by $\overline{P}$ in the frequency domain. In equation (8), the $(4\pi)^2|\mathbf{x}_0|^2$ factor compensates for power attenuation while the complex exponential compensates for what is called "range offset". Equations (7) and equation (8), alike, are known as the Fourier Diffraction theorem (FDT) for radar imaging, which states that the radar received signal scattered from a target scene is proportional to the three-dimensional Fourier transform of its reflectivity function evaluated at $-2k\widehat{\mathbf{x}_0}$. The transmitted signal P is band-limited with a support band given by the set $\left\{f_c - \frac{B}{2}, f_c + \frac{B}{2}\right\}$, where B is the signal bandwidth, and is usually chosen so that its power spectrum is given by $|P(f)|^2 \approx \text{rect}\left(\frac{f-f_c}{B}\right)$. Thus the FDT reveals that each radar signal gives the three-dimensional Fourier transform of the target reflectivity evaluated on the finite line-segment determined by $\mathbf{K} = -2k\widehat{\mathbf{x}_0}$, $f \in \left[f_c - \frac{B}{2}, f_c + \frac{B}{2}\right]$. Consequently, the object in radar imaging is to populate the wave number domain with as much data as needed to reconstruct the reflectivity function V.

B. Two-Dimensional Turntable ISAR Imaging

In Synthetic Aperture Radar (SAR) imaging, a stationary target scene is imaged via numerous radar returns measured along some sort of flight path. A changing sensor position corresponds to a changing $\widehat{\mathbf{x}_0}$, which results in a means of populating the wave number domain according to the FDT. In ISAR, a stationary radar sensor measures numerous returns scattered from a moving target, which is also mathematically equivalent to a changing sensor location $\widehat{\mathbf{x}_0}$, if the origin of the coordinate system is placed at the center of the moving target scene. In a turntable ISAR imaging setup[2] the target scene is rotated counter-clockwise about the x_3-axis by ϕ radians. If we were to let q denote a stationary scattering density, then we have $V(\mathbf{x}) = q\left(\mathcal{R}_1^{-1}(\phi)\mathbf{x}\right)$[3], where it can be found that the rotational matrix $\mathcal{R}_1$ is given by

$$\mathcal{R}_1(\phi) = \begin{pmatrix} \cos\phi & -\sin\phi & 0 \\ \sin\phi & \cos\phi & 0 \\ 0 & 0 & 1 \end{pmatrix}. \quad (9)$$

One can check that for every $\phi \in [0, 2\pi]$, $\mathcal{R}_1$ is an orthogonal transformation (i.e. $\mathcal{R}_1^{-1}$ exists and $\mathcal{R}_1^{-1} = \mathcal{R}_1^T$). For each value of ϕ the data set recorded by the ISAR system is given by

$$\begin{aligned} D(f) &= |P(f)|^2 \int_{\mathbb{R}^3} q\left(\mathcal{R}_1^{-1}\mathbf{z}\right) e^{i2k\widehat{\mathbf{x}_0}\cdot\mathbf{z}} d\mathbf{z} \\ &= |P(f)|^2 \int_{\mathbb{R}^3} q(\mathbf{y}) e^{i2k\widehat{\mathbf{x}_0}\cdot\mathcal{R}_1\mathbf{y}} d\mathbf{y} \\ &= |P(f)|^2 \int_{\mathbb{R}^3} q(\mathbf{y}) e^{i2k\mathcal{R}_1^{-1}\widehat{\mathbf{x}_0}\cdot\mathbf{y}} d\mathbf{y} \\ &= |P(f)|^2 \mathcal{F}_3\{q\}(\mathbf{K}), \end{aligned} \quad (10)$$

where $\mathbf{K} = -2k\mathcal{R}_1^{-1}\widehat{\mathbf{x}_0}$. To understand what is happening in the wave number domain, we assume that the target scene is to be rotated clock-wise, and take $\widehat{\mathbf{x}_0} = (1,0,0)^{\text{T}}$. Thus, if $\tilde{k} = -2k$, then $\mathbf{K} = (K_1, K_2, K_3)^{\text{T}} = (\tilde{k}\cos\phi, \tilde{k}\sin\phi, 0)^{\text{T}}$, and the signal in the (f,ϕ) space is determined by:

$$\tilde{D}(f,\phi) = |P(f)|^2 \mathcal{F}_2\{\tilde{q}\}\left(\tilde{k}\boldsymbol{\mu}\right), \quad (11)$$

[2]Many turntable radar setups have a bi-static configuration. That is the transmitter and the receiver are generally located at two different positions in the system geometry. It is usually the case that system configuration can be modified so that the antenna range to any target on the turntable is approximately the same for both the transmitter and receiver.

[3]Note that the use of $\mathcal{R}_1^{-1}$, rather than $\mathcal{R}_1$, corresponds to counter clockwise turntable rotation.

978-1-4673-0658-4/12/$31.00 ©2012 IEEE

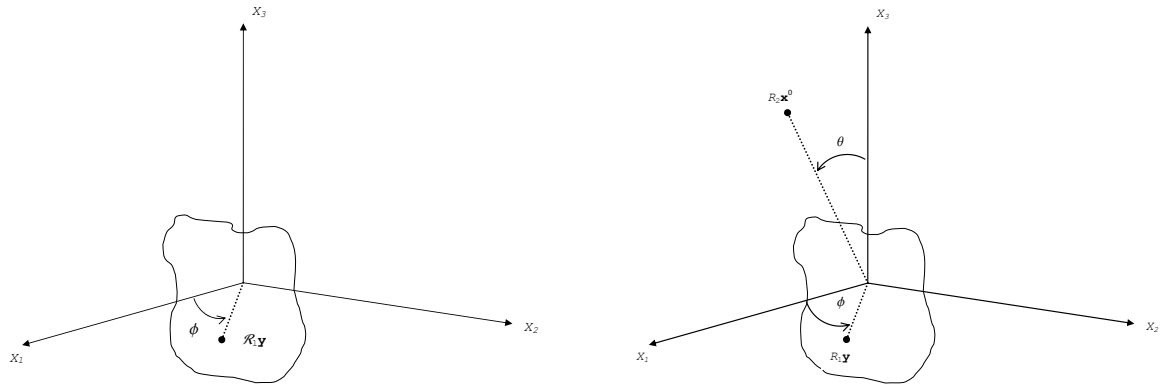

(a) 2-D Turntable Geometry.

(b) 3-D Turntable Geometry.

Fig. 1.

where $\mathcal{F}_2\{h\}(\Omega)$ denotes the two-dimensional Fourier transform of h evaluated at the point Ω in 2D Fourier space, $\tilde{q}(y_1, y_2) = \int q(y_1, y_2, y_3)dy_3$ is the projection of q onto the $x_1 - x_2$ axis, and $\boldsymbol{\mu} = (\cos\phi, \sin\phi)^{\mathrm{T}}$. Note that the vector $\boldsymbol{\mu}$ is an element of the unit circle S^1 (the set of all unit vectors in $\mathbb{R}^2$). The data $\tilde{D}$ can be sampled over a two-dimensional Cartesian grid, allowing us to form a 2D image via an inverse 2D spatial Fourier transform:

$$I(\mathbf{x}) = \frac{1}{(2\pi)^2}\int E(K_1, K_2)e^{iK_1x_1}e^{iK_2x_2}dK_1dK_2, \quad (12)$$

where E is the wave number data sampled over a Cartesian data grid.

For many SAR applications, Polar Formatting can be used to produce an image. In this case, the received data is sample at a variety of different angles. This data is used to populate a polar raster in the Wave Number Domain. Next, this data is interpolated onto a two dimensional rectangular grid. Finally, a 2-D IFFT is applied to the interpolated data in order to produce the final image.

C. Three-Dimensional Turntable ISAR Imaging

If in the previous turntable setup we also rotate the radar antenna about the x_2 axis by θ radians, we have that the new antenna position is given by $\mathcal{R}_2(\theta)\mathbf{x}_0$, where:

$$\mathcal{R}_2(\theta) = \begin{pmatrix} \cos\theta & 0 & \sin\theta \\ 0 & 1 & 0 \\ -\sin\theta & 0 & \cos\theta \end{pmatrix}. \quad (13)$$

This implies that the data set recorded by the ISAR system is then determined by

$$\begin{aligned} D(f) &= |P(f)|^2 \int_{\mathbb{R}^3} q\left(\mathcal{R}_1^{-1}(\phi)\mathbf{z}\right) e^{i2k\widehat{\mathcal{R}_2(\theta)\mathbf{x}_0}\cdot\mathbf{z}}d\mathbf{z} \\ &= |P(f)|^2 \mathcal{F}_3\{q\}(\mathbf{K}), \end{aligned} \quad (14)$$

where $\mathbf{K} = -2k\mathcal{O}(\phi,\theta)\widehat{\mathbf{x}}_0$, and $\mathcal{O}(\phi,\theta) = \left(\mathcal{R}_1^{-1}\mathcal{R}_2\right)(\phi,\theta)$. If we let $\widehat{\mathbf{x}_0} = (0,0,1)^{\mathrm{T}}$ (that is the initial antenna position is located on the x_3 axis) we see that

$$\mathbf{K} = \begin{pmatrix} K_1 \\ K_2 \\ K_3 \end{pmatrix} = \begin{pmatrix} \tilde{k}\cos\phi\sin\theta \\ \tilde{k}\sin\phi\sin\theta \\ \tilde{k}\cos\theta \end{pmatrix} = \tilde{k}\boldsymbol{\mu}, \quad (15)$$

where $\boldsymbol{\mu} = (\cos\phi\sin\theta, \sin\phi\sin\theta, \cos\theta)^{\mathrm{T}}$ is an element of the unit sphere S^2 (the set of all unit vectors in $\mathbb{R}^3$). Thus the $\mathbf{K}$-domain data takes up a three-dimensional space, allowing us to form a 3D image via an inverse 3D Fourier transform:

$$I(\mathbf{x}) = \frac{1}{(2\pi)^3}\int E(\mathbf{K})e^{i\mathbf{K}\cdot\mathbf{x}}d\mathbf{K}. \quad (16)$$

III. FILTERED-ADJOINT IMAGING

The framework for a filtered back projection ISAR imaging algorithm is given in this section. Recall that the received ISAR signal, S, is a function of both frequency, f, and angle, $\boldsymbol{\mu}$. We will further assume that S is a member of $L^2(C^m)$, the space of square-integrable functions on the unit cylinder $C^m = \mathbb{R}\times S^{m-1}$. Here $m = 2$ or $m = 3$, corresponding to the number of imaging dimensions. In either case we can write the reflectivity function in terms of a rotating scattering density function:

$$V(\mathbf{x}) = q\left(\mathcal{O}_m\mathbf{x}\right). \quad (17)$$

When $m = 2$, we have $\mathcal{O}_m = \mathcal{R}_1^{-1}$, and when $m = 3$, we have $\mathcal{O}_m = \mathcal{R}_1^{-1}\mathcal{R}_2$, where $\mathcal{R}_1$ and $\mathcal{R}_2$ are the orthogonal linear transformations given in the previous section. According to equation (4), this implies that the ISAR signal is given by:

$$S(f) = P(f)\int_{\mathbb{R}^3} q(\mathbf{y})\frac{e^{-i2k|\mathbf{y}-\mathcal{O}_m\mathbf{x}_0|}}{(4\pi)^2|\mathbf{y}-\mathcal{O}_m\mathbf{x}_0|^2}d\mathbf{y} \quad (18)$$

A. The ISAR Back Projection Operator

If we let r_a denote the distance of the radar sensor to the scene center, then for $m = 2$ we let $\mathbf{x}_0 = (r_a, 0, 0)^{\mathrm{T}}$. Thus we can write $\mathcal{O}_m\mathbf{x}_0 = r_a\boldsymbol{\mu}$, where $\boldsymbol{\mu}\in S^1$. Likewise, for $m = 3$ we let $\mathbf{x}_0 = (0,0,r_a)^{\mathrm{T}}$ so that we can write $\mathcal{O}_m\mathbf{x}_0 = R_a\boldsymbol{\mu}$, where $\boldsymbol{\mu}\in S^2$. In either case equation (18) can be written as:

$$S(f,\boldsymbol{\mu}) = F_m\{q\}(f,\boldsymbol{\mu}), \quad (19)$$

where

$$F_m\{q\}(f,\boldsymbol{\mu}) = \int_{\mathbb{R}^3} q(\mathbf{y}) e^{-i2kR_m(\mathbf{y},\boldsymbol{\mu})} A_m(f,\boldsymbol{\mu},\mathbf{y}) d\mathbf{y}, \tag{20}$$

$$\mathbf{R}_m(\mathbf{z},\boldsymbol{\mu}) = \begin{cases} \mathbf{z} - R_a(\boldsymbol{\mu},0)^{\mathrm{T}}, & \text{if} \quad m=2 \\ \mathbf{z} - R_a\boldsymbol{\mu}, & \text{if} \quad m=3, \end{cases} \tag{21}$$

$$A_m(f,\boldsymbol{\mu},\mathbf{y}) = \frac{P(f)}{(4\pi)^2 \left(R_m(\mathbf{y},\boldsymbol{\mu})\right)^2}, \tag{22}$$

and $R_m(\mathbf{z},\boldsymbol{\mu}) = |\mathbf{R}_m(\mathbf{z},\boldsymbol{\mu})|$. Note that we have used the symbol F to denote the forward ISAR Fourier Integral Operator (FIO). A derivation of the formal adjoint of this FIO is now in order. For functions $G, H \in L^2(C^m)$, define the inner product (G,H), by:

$$(G,H)_m = \int_{S^{m-1}} \int_{\mathbb{R}} G(f,\boldsymbol{\mu}) \overline{H(f,\boldsymbol{\mu})} df d\boldsymbol{\mu}, \tag{23}$$

and recall the Hermitian inner product on $L^2(\mathbb{R}^3)$:

$$\langle g,h \rangle = \int_{\mathbb{R}^3} g(\mathbf{x}) \overline{h(\mathbf{x})} d\mathbf{x}, \quad g,h \in L^2(\mathbb{R}^3) \tag{24}$$

Define the operator $\mathcal{B}_m$ on $L^2(C^m)$, by:

$$\mathcal{B}_m\{H\}(\mathbf{x}) = \int_{S^{m-1}} \int_{\mathbb{R}} H(f,\boldsymbol{\mu}) \overline{A_m(f,\boldsymbol{\mu},\mathbf{x})} e^{i2kR_m(\mathbf{x},\boldsymbol{\mu})} df d\boldsymbol{\mu}. \tag{25}$$

A quick application of Fubini's theorem shows that $\mathcal{B}_m = F_m^\dagger$ on $L^2(C^m)$. That is for $g \in L^2(\mathbb{R}^3)$ and $H \in L^2(C^m)$, then $(F_m g, H)_m = \langle g, \mathcal{B}_m H \rangle$, thus making $\mathcal{B}_m$ our ISAR back projection operator. We now seek to form an image I via:

$$I(\mathbf{x}) = (\mathcal{B}_m \mathcal{Q}_m)\{S\}(\mathbf{x}) = \int_{S^{m-1}} \int_0^\infty S(f,\boldsymbol{\mu}) \mathcal{Q}_m(f,\boldsymbol{\mu},\mathbf{x}) \overline{A_m(f,\boldsymbol{\mu},\mathbf{x})} e^{i2kR_m(\mathbf{x},\boldsymbol{\mu})} df d\boldsymbol{\mu}, \tag{26}$$

where $\mathcal{Q}_m$ is a filter acting on S. The goal of the next two sections is to evaluate this filter using the method of Stationary Phase.

B. Point Spread Function Analysis using the Stationary Phase Method

In order to lighten the processing load of an imaging algorithm most radar systems make use of quadrature sampling which has the useful property of converting a real signal into a complex signal. Since the carrier frequency of a radar signal is usually chosen to be larger than half of the transmitted signal bandwidth, the signal's support band is a subset of the positive half plane. This means that we can assume that the ISAR system is operating on only positive frequencies. Then, substituting the expression for the received signal (19) into equation (26) provides yields the following expression for the image:

$$I(\mathbf{x}) = \int_{\mathbb{R}^3} q(\mathbf{y}) K(\mathbf{x},\mathbf{y}) d\mathbf{y}, \tag{27}$$

where the point spread function (PSF), K is given by:

$$K(\mathbf{x},\mathbf{y}) = \int_{S^{m-1}} \int_0^\infty e^{i\varphi(f,\boldsymbol{\mu},\mathbf{x},\mathbf{y})} a(f,\boldsymbol{\mu},\mathbf{x},\mathbf{y}) df d\boldsymbol{\mu}, \tag{28}$$

where $\varphi(f,\boldsymbol{\mu},\mathbf{x},\mathbf{y}) = 2k\left[R_m(\mathbf{x},\boldsymbol{\mu}) - R_m(\mathbf{y},\boldsymbol{\mu})\right]$ and $a(f,\boldsymbol{\mu},\mathbf{x},\mathbf{y}) = (\overline{A}_m \mathcal{Q}_m A_m)(f,\boldsymbol{\mu},\mathbf{x},\mathbf{y})$. In order to obtain an exact inversion formula, we must have:

$$K(\mathbf{x},\mathbf{y}) = \delta(\mathbf{x}-\mathbf{y}) = \frac{1}{(2\pi)^m} \int_{\mathbb{R}^m} e^{i(\mathbf{x}-\mathbf{y})\cdot\boldsymbol{\xi}} d\boldsymbol{\xi} \tag{29}$$

Note that this would require the phase function φ to have a single non-degenerate critical point at $\mathbf{y} = \mathbf{x}$. That is, $\nabla_m \varphi(f,\boldsymbol{\mu},\mathbf{x},\mathbf{y})|_{\mathbf{y}=\mathbf{x}} = \mathbf{0}$ such that the Hessian matrix $D_m^2 \varphi$ is nonsingular, according to the stationary phase theorem[22]. Here, the gradient operator in polar/spherical coordinates is given by $\nabla_m = \frac{\partial}{\partial f}\widehat{\mathbf{f}} + \frac{\partial_m}{\partial \boldsymbol{\mu}}$, and

$$\frac{\partial}{\partial \boldsymbol{\mu}} = \begin{cases} \frac{1}{f}\frac{\partial}{\partial \phi}\widehat{\boldsymbol{\phi}}, & \text{if} \quad m=2 \\ \frac{1}{f}\frac{\partial_m}{\partial \theta}\widehat{\boldsymbol{\theta}} + \frac{1}{f\sin\theta}\frac{\partial}{\partial \phi}\widehat{\boldsymbol{\phi}}, & \text{if} \quad m=3 \end{cases} \tag{30}$$

We first make a change of variables, $f = \beta f'$, where $\beta > 0$:

$$K(\mathbf{x},\mathbf{y}) = \beta \int_{S^{m-1}} \int_0^\infty e^{i\beta\varphi'(f',\boldsymbol{\mu},\mathbf{x},\mathbf{y})} a'(f',\boldsymbol{\mu},\mathbf{x},\mathbf{y}) df' d\boldsymbol{\mu}, \tag{31}$$

where $\varphi'(f',\boldsymbol{\mu},\mathbf{x},\mathbf{y}) = \frac{4\pi f'}{c}\left[R_m(\mathbf{x},\boldsymbol{\mu}) - R_m(\mathbf{y},\boldsymbol{\mu})\right]$ and $a'(f',\boldsymbol{\mu},\mathbf{x},\mathbf{y}) = a(\beta f',\boldsymbol{\mu},\mathbf{x},\mathbf{y})$. We then apply the modified gradient operator, $\nabla_m = \frac{\partial}{\partial f'}\widehat{\mathbf{f}}' + \frac{\partial_m}{\partial \boldsymbol{\mu}}$, to the phase φ. In either case for m, we have that the major contribution for large β comes from the critical points described by

$$\frac{\partial}{\partial f'}\varphi'(f',\boldsymbol{\mu},\mathbf{x},\mathbf{y}) = \frac{4\pi}{c}\left[R_m(\mathbf{x},\boldsymbol{\mu}) - R_m(\mathbf{y},\boldsymbol{\mu})\right] = 0 \tag{32}$$

$$\frac{\partial_m}{\partial \boldsymbol{\mu}}\varphi'(f',\boldsymbol{\mu},\mathbf{x},\mathbf{y}) = \frac{4\pi f'}{c}\left[\widehat{\mathbf{R}}_m(\mathbf{x},\boldsymbol{\mu}) - \widehat{\mathbf{R}}_m(\mathbf{y},\boldsymbol{\mu})\right] \cdot \frac{\partial_m}{\partial \boldsymbol{\mu}}(\mathcal{O}_m \mathbf{x}_0) = 0 \tag{33}$$

The first equation tells us that the distance from the antenna to the target located at $\mathbf{x}$ must be the same as the distance to the target located at $\mathbf{y}$. The second equation tells us that the range rate (giving rise to a Doppler shift) must be the same for $\mathbf{x}$ and $\mathbf{y}$. Thus we have the familiar idea of locating a target from its range and Doppler shift[7].

C. Evaluating the Filter $\mathcal{Q}$

In Cartesian coordinates (i.e. making the change of variables: $\boldsymbol{\eta} = f\boldsymbol{\mu}$), we have that equation (28):

$$K(\mathbf{x},\mathbf{y}) = \int_{\mathbb{R}^m} e^{i\varphi''(\boldsymbol{\eta},\mathbf{x},\mathbf{y})} a''(\boldsymbol{\eta},\mathbf{x},\mathbf{y}) d\boldsymbol{\eta}, \tag{34}$$

where $\varphi''(\boldsymbol{\eta},\mathbf{x},\mathbf{y}) = \varphi(\eta,\widehat{\boldsymbol{\eta}},\mathbf{x},\mathbf{y})$ and $a''(\boldsymbol{\eta},\mathbf{x},\mathbf{y}) = \eta^{1-m} a(\eta,\widehat{\boldsymbol{\eta}},\mathbf{x},\mathbf{y})$, where $\eta = |\boldsymbol{\eta}|$ and $\widehat{\boldsymbol{\eta}} = \frac{\boldsymbol{\eta}}{\eta}$. Note that:

$$\begin{aligned} \varphi''(\boldsymbol{\eta},\mathbf{x},\mathbf{y}) &= \frac{4\pi\eta}{c}\int_0^1 \frac{d}{d\lambda}\, R_m(\mathbf{x},\widehat{\boldsymbol{\eta}})|_{\mathbf{x}=\mathbf{y}+\lambda(\mathbf{x}-\mathbf{y})}\, d\lambda \\ &= (\mathbf{x}-\mathbf{y})\cdot\Xi(\boldsymbol{\eta},\mathbf{x},\mathbf{y}), \\ \Xi(\boldsymbol{\eta},\mathbf{x},\mathbf{y}) &= \frac{4\pi\eta}{c}\int_0^1 \nabla_{\mathbf{x}}\, R_m(\mathbf{x},\widehat{\boldsymbol{\eta}})|_{\mathbf{x}=\mathbf{y}+\lambda(\mathbf{x}-\mathbf{y})}\, d\lambda \end{aligned} \tag{35}$$

Introducing the change of variables, $\boldsymbol{\xi} = \Xi(\boldsymbol{\eta},\mathbf{x},\mathbf{y})$, then we have:

$$K(\mathbf{x},\mathbf{y}) = \int_{\mathbb{R}^m} e^{i(\mathbf{x}-\mathbf{y})\cdot\boldsymbol{\xi}} a''(\boldsymbol{\eta}(\boldsymbol{\xi}),\mathbf{x},\mathbf{y}) \left|\frac{\partial\boldsymbol{\eta}}{\partial\boldsymbol{\xi}}\right| d\boldsymbol{\xi}, \tag{36}$$

978-1-4673-0658-4/12/$31.00 ©2012 IEEE

where $\left|\frac{\partial \boldsymbol{\eta}}{\partial \boldsymbol{\xi}}\right|$ is the Jacobian determinant resulting from the change of variables. If we note that

$$a''(\boldsymbol{\eta}(\boldsymbol{\xi}), \mathbf{x}, \mathbf{y}) = (\eta(\boldsymbol{\xi}))^{1-m}(\overline{A}_m \mathcal{Q}_m A_m)(f(\boldsymbol{\xi}), \boldsymbol{\mu}(\boldsymbol{\xi}), \mathbf{x}, \mathbf{y}), \tag{37}$$

we see that we can approximate the PSF for exact inversion in equation (29) by letting

$$\mathcal{Q}_m(f, \boldsymbol{\mu}, \mathbf{x}) = \frac{(4\pi)^4 (R_m(\mathbf{x}, \boldsymbol{\mu}))^4 f^{m-1}}{|P(f)|^2 \left|\left(\frac{\partial \boldsymbol{\eta}}{\partial \boldsymbol{\xi}}\right)(f, \boldsymbol{\mu})\right|} \chi(f, \boldsymbol{\mu}), \tag{38}$$

where $\chi(\mathbf{x}, f\boldsymbol{\mu})$ is a smooth cutoff function that prevents from dividing by zero. Given the ISAR data set $S(f, \boldsymbol{\mu})$, note that applying the proposed FBP operation to the data set is mathematically equivalent to the following imaging operation:

$$I(\mathbf{x}) = \int_{S^{m-1}} \int_0^\infty S(f, \boldsymbol{\mu}) \Psi(f, \boldsymbol{\mu}, \mathbf{x}) df d\boldsymbol{\mu}, \tag{39}$$

where

$$\Psi(f, \boldsymbol{\mu}, \mathbf{x}) = \frac{(4\pi)^2 (R_m(\mathbf{x}, \boldsymbol{\mu}))^2 f^{m-1}}{P(f) \left|\left(\frac{\partial \boldsymbol{\eta}}{\partial \boldsymbol{\xi}}\right)(f, \boldsymbol{\mu})\right|} \chi(f, \boldsymbol{\mu}) e^{i2kR_m(\mathbf{x}, \boldsymbol{\mu})} \tag{40}$$

takes on the form of a general "focusing" operator for Spherical Wave ISAR (SWISAR)[3], [10], [25]. Thus, the proposed inversion scheme has immediate applications for near-field configurations. The $(P(f))^{-1}$ term in equation (41) refers to what is known as a source deconvolution operation for the range imaging problem[20], and can be replaced by $\overline{P(f)}$ for imaging systems that make use of matched filtering. Under these assumptions, the focusing operator becomes

$$\Psi(f, \boldsymbol{\mu}, \mathbf{x}) = (4\pi)^2 (R_m(\mathbf{x}, \boldsymbol{\mu}))^2 f^{m-1} \overline{P(f)} e^{i2kR_m(\mathbf{x}, \boldsymbol{\mu})}. \tag{41}$$

IV. The FBP and CBP Algorithms

In general, filtered back projection (FBP) imaging schemes are commonly used for forming images from radar data. FBP algorithms were originally used in back projection tomography. The mathematical basis of these algorithms is Radon transform inversion, where the measured returns are related to the projection/path integral of the object reflectivity function. Back projection in synthetic aperture radar is often considerably less efficient than other common inversion algorithms, such as the Polar Format Algorithm.

Assume that a set of turntable radar data is already given as a series of range profiles. For simplicity, the focusing operator approach can be applied to form an image, as is indicated by equation (41). Now, when $m = 3$, it can be assumed that $\boldsymbol{\mu} = \boldsymbol{\mu}(\theta, \phi)$. Then, the integral in equation (39) can be written in three dimensional spherical coordinates as follows.

$$I(\mathbf{x}) = \int_0^{2\pi} \int_0^\pi \int_0^\infty S(f, \theta, \phi) \Psi(f, \theta, \phi, \mathbf{x}) \sin\theta df d\theta d\phi \tag{42}$$

Here the focusing operater in Ψ given in equation (41) can be rewritten as

$$\Psi(f, \phi, \mathbf{x}) = (4\pi)^2 (R(\mathbf{x}, \theta, \phi))^2 f^2 \overline{P(f)} e^{i2kR(\mathbf{x}, \theta, \phi)} \tag{43}$$

Now, the received signal in equation (42) can be combined with the matched filtering factor $\overline{P(f)}$ to form a pulse compressed version of the signal given by $D(f, \theta, \phi) = (4\pi)^2 \overline{P(f)} S(f, \theta, \phi)$.

$$I(\mathbf{x}) = \int_0^\infty \int_0^\pi \int_0^{2\pi} f^2 D(f, \theta, \phi) (R(\mathbf{x}, \theta, \phi))^2 \times e^{i2kR(\mathbf{x}, \theta, \phi)} \sin\theta d\phi d\theta df \tag{44}$$

Given that $\mathbf{x} = (x_1, x_2, x_3)^T$, the range variable $R(\mathbf{x}, \theta, \phi)$ can be reperented in acordance with equation (21).

$$\mathbf{R}(\mathbf{x}, \theta, \phi) = \begin{pmatrix} x_1 - R_a sin\theta cos\phi \\ x_2 - R_a sin\theta \sin\phi \\ x_3 - R_a cos\theta) \end{pmatrix} \tag{45}$$

In polar coordinates, the range for a given value of $\mathbf{x} = |\mathbf{x}|(sin\tilde{\theta}cos\tilde{\phi}, \sin\tilde{\theta}\sin\tilde{\phi}, \cos\tilde{\phi})^T$ is given in terms of the following vector.

$$\mathbf{R}(\mathbf{x}, \theta, \phi) = \begin{pmatrix} |\mathbf{x}| sin\tilde{\theta}cos\tilde{\phi} - R_a sin\theta cos\phi \\ |\mathbf{x}| sin\tilde{\theta}sin\tilde{\phi} - R_a sin\theta sin\phi \\ |\mathbf{x}| cos\tilde{\theta} - R_a cos\theta \end{pmatrix} \tag{46}$$

Evaluating the norm of the vector, given in the equation above, gives

$$\begin{aligned} R(\mathbf{x}, \theta, \phi) = \sqrt{|\mathbf{x}|^2 + R_a^2 - R_a \mathbf{x} \cdot \boldsymbol{\mu}}, \quad \boldsymbol{\mu} = \boldsymbol{\mu}(\theta, \phi), \\ \mathbf{x} \cdot \boldsymbol{\mu} = |\mathbf{x}| \cos\tilde{\theta} \cos\theta - |\mathbf{x}| \sin\tilde{\theta} \sin\theta \cos(\tilde{\phi} - \phi) \end{aligned} \tag{47}$$

After replacing $\tilde{\phi}$ with ψ, the inner integral becomes a circular convolution.

$$I(\mathbf{x}) = \int_0^\infty f^2 \int_0^\pi Q(f, \mathbf{x}, \theta, \psi) \sin\theta d\theta df, \tag{48}$$

where

$$\begin{aligned} Q(\mathbf{x}, \theta, \psi) = (D *_\phi T)(\mathbf{x}, \theta, \psi), \\ (D *_\phi T)(\mathbf{x}, \theta, \psi) = \int_0^{2\pi} D(f, \theta, \psi - \phi) T(f, \mathbf{x}, \theta, \phi) d\phi, \end{aligned} \tag{49}$$

and

$$T(f, \mathbf{x}, \theta, \phi) = (R(\mathbf{x}, \theta, \phi))^2 e^{\frac{4\pi i f}{c_0} R(\mathbf{x}, \theta, \phi)} \tag{50}$$

The convolution in the equation above can be computed using the identity $f * g = \mathcal{F}^{-1}\{\mathcal{F}\{f\}\mathcal{F}\{g\}\}$. In the case where a discrete data set is given in place of a continious function, the Fourier Transform and the Inverse Fourier Transform can be replaced with the FFT and the IFFT respectively. Thus, in the discrete case, Q is given by:

$$Q(f, \mathbf{x}, \theta, \psi) = \text{IFFT}_\phi\{\text{FFT}_\phi\{D\} \cdot \text{FFT}_\phi\{T\}\}(f, \mathbf{x}, \theta, \psi) \tag{51}$$

The FFT is applied over N_p sample points. Now, let N_f denote the number of samples of the frequency variable f. Then, assuming that θ can be sampled over N_s sample points, the descrete versions of f and θ can be denoted by:

$$\begin{aligned} f_j = f_{min} + j\Delta f \text{ where } j = 1, 2, \ldots N_f \\ \theta_k = \theta_{min} + k\Delta\theta \text{ where } k = 1, 2, \ldots N_s \end{aligned} \tag{52}$$

978-1-4673-0658-4/12/$31.00 ©2012 IEEE

Then, the discrete version of the image function given in equation (48) can be found using weighted sums in terms of f_j and θ_k.

$$I(\mathbf{x}) = \frac{1}{N_f N_p} \sum_{j=1}^{N_f} \sum_{k=1}^{N_p} f_j^2 Q(\mathbf{x}, j, k) \sin \theta_k \qquad (53)$$

The formulations in this paper provides a Mathematical framework that can be used to developed a 3-dimensional turntable imaging algorithm. Future work will center on developing a working CBP algorithm for 3-dimensional turntable SAR. This algorithm will operate on a set of SAR data in the form of range profiles. Once pulse compression is applied to the received data, a circular convolution and weighted sums will be applied. There are several other steps that need to be included in this algorithm, including an interpolation step and range compensation.

V. CONCLUSIONS

In this paper, we have provided a filtered back projection inversion method for mono-static ISAR radar imaging. In order to achieve this we have derived a forward integral operator model for the forward ISAR problem, and evaluated its formal adjoint (back projection operator) in the signal function space. Applying the stationary phase method to our inversion procedure, we have shown that the filtered back projection data approximates the desired target reflectivity function with large system bandwidth. One of the advantages in the filtered back projection approach is that there is no need of employing a far-field approximation for the radar data. Thus our approach makes this filtered back projection method ideal for near-field imaging. Although no numerical results are provided in the paper to demonstrate this, it is shown that the FBP scheme reduces to similar results for near-field turntable radar imaging which have been proven to be efficient in ISAR image formation. We will realize numerical results in both 2D and 3D very soon.

ACKNOWLEGMENTS

This work was partially supported by the US Department of Defense Army Research Office under grant number *W911NF-08-1-0511*, and by the Norman Hackerman Advanced Research Program under grant number *003599-0001-2009*.

REFERENCES

[1] Ausherman, D. A., Kozma, A., Walker, J. L., Jones, H. M., Poggio, E. C., "Developments in Radar Imaging," IEEE Transactions on Aerospace and Electronic Systems Vol. AES-20 No. 4 (1984) 363-400

[2] Born, M., Wolf, E. *Principles of Optics: Electromagnetic Theory of Propagation, Interference and Diffraction of Light (7th Edition)*. Cambridge: Cambridge University Press, 1999

[3] Broquetas, A., Palau, J., Jofre, L., Cardama, A., "Spherical Wave Near-Field Imaging and Radar Cross-Section Measurement," IEEE Transactions on Antennas and Propagation Vol. 46 No. 5 (1998) 730-735

[4] Carrara, W. G., Goodman, R. S., Majewski, R. M., *Spotlight Synthetic Aperture Radar Signal Processing Algorithms*. Boston: Artech House Inc., 1995

[5] Chen, C. C., Andrews, H. C., "Multifrequency Imaging of Radar Turntable Data," IEEE Transactions on Aerospace and Electronic Systems Vol. AES-16 No.1 (1980) 15-22

[6] Cheney, M., Borden, B., "Microlocal structure of inverse synthetic aperture radar data," Inverse Problems **19** (2003) 173193

[7] Cheney, M., Borden, B., *Fundamentals of Radar Imaging*. Philadelphia: SIAM, 2009

[8] Curlander, J. C., McDonough, R. N., *Synthetic Aperture Radar Systems and Signal Processing*. New York: John Wiley & Sons Inc., 1991

[9] Deming, R. W., "Tutorial on Fourier space coverage for scattering experiments, with application to SAR," Proceedings of SPIE Volume 7699 Algorithms for Synthetic Aperture Radar Imagery XVII (2010)

[10] Fortuny, J., "An Efficient 3-D Near-Field ISAR Algorithm," IEEE Transactions on Aerospace and Electronic Systems Vol. 34 No. 4 (1998) 1261-1269

[11] Garza, G., Lopez J. X., Qiao Z., Cross-Range Imaging of SAR Data, Pacific Journal of Applied Mathematics, 2(2009), 65-81

[12] Jakowatz, C.,Wahl, D., Eichel, P., Ghiglia, D.,Thompson, P., *Spotlight-Mode Synthetic Aperture Radar: A Signal Processing Approach*, Norwell, MA: Kluwer Academic Publishers, 1996

[13] Kempf, T., Peichl, M., Dill, S., Suess, H., "3D Tower-Turntable ISAR Imaging," Proceeding of the 4th European Radar Conference (2007) 114-117

[14] Lopez J. X., Garza, G., Qiao Z., Cross-range imaging of SAR and PDE analysis, Proc. of SPIE Vol. 7698 (2010) 76981C-1-76981C-15

[15] Lopez, J. X., Qiao, Z., "Filtered Back Projection Inversion of Turntable ISAR Data," Proc. of SPIE Volume: 8051 (2011) 805109-1 - 805109-9

[16] Lopez, J. X., *Inverse Synthetic Aperture Radar Imaging Theory and Applications*. MS Thesis. The University of Texas-Pan American, Edinburg, TX (2011)

[17] Nolan, C. J., Cheney, M., "Synthetic Aperture Inversion," Inverse Problems **18** (2002) 221-235

[18] Prickett, M. J., Chen, C. C., "Principles of Inverse Synthetic Aperture Radar (ISAR) Imaging," EASCON '80; Electronics and Aerospace Systems Conference (1980) 340-345

[19] Liu, F., Nashed Z., Nguerekata G., Pokrajac D., Qiao Z., et al, Advances in Applied and Computational Mathematics, Nova Science Publication, Inc., USA, 2006

[20] Soumekh, M. *Synthetic Aperture Radar Signal Processing with MATLAB Algorithms*. New York: Wiley-Interscience, 1999

[21] Stein, E. M., Weiss, G. *Introduction to Fourier Analysis on Euclidean Spaces*. Princeton: Princeton University Press, 1971

[22] Stein, E. M., Weiss, G. *Harmonic Analysis: Real-variable Methods, Orthogonality and Oscillatory Integrals*. Princeton: Princeton University Press, 1993

[23] Stratton, J. A., *Electromagnetic Theory*. New Jersey: John Wiley & Sons, Inc., 2007

[24] van Zyl, M.W., Inggs, M.R., "Inverse Synthetic Aperture Radar Images of Moving Targets," IEEE South African Symposium on Communications and Signal Processing (1991) 42-46

[25] Vaupel, T., Eibert, T. F., "Comparison and Application of Near-field ISAR Imaging Techniques for Far-field Radar Cross Section Determination," IEEE Transactions on Atennas and Propagation Vol. 54 No. 1 (2006) 144-151

[26] Yazici, B., Cheney, M., Yarmen, C. E., "Synthetic-aperture inversion in the presence of noise and clutter" Inverse Problems **22** (2006) 1705-1729